Antiferroelectric-to-Ferroelectric Switching in $CH_3NH_3PbI_3$ Perovskite and Its Potential Role in Effective Charge Separation in Perovskite Solar Cells

Galhenage A. Sewvandi,[1,2,†] Dengwei Hu,[2,3] Changdong Chen,[2] Hao Ma,[2] Takafumi Kusunose,[2] Yasuhiro Tanaka,[2] Shunsuke Nakanishi,[2] and Qi Feng[2,*]

[1]*Department of Materials Science and Engineering, Faculty of Engineering, University of Moratuwa, Katubedda 10400, Sri Lanka*

[2]*Department of Advanced Materials Science, Faculty of Engineering, Kagawa University, 2217-20 Hayashi-cho, Takamatsu 761-0396, Japan*

[3]*College of Chemistry and Chemical Engineering, Engineering Research Center of Advanced Ferroelectric Functional Materials, Key Laboratory of Photochemistry of Shaanxi Province, Baoji University of Arts and Science, 1 Hi-Tech Avenue, Baoji, Shaanxi 721013, People's Republic of China*

(Received 9 April 2016; revised manuscript received 31 May 2016; published 11 August 2016)

Perovskite solar cells (PSCs) often suffer from large performance variations which impede to define a clear charge-transfer mechanism. Ferroelectric polarization is measured numerically using $CH_3NH_3PbI_3$ ($MAPbI_3$) pellets to overcome the measurement issues such as pinholes and low uniformity of thickness, etc., with $MAPbI_3$ thin films. $MAPbI_3$ perovskite is an antiferroelectric semiconductor which is different from typical semiconducting materials and ferroelectric materials. The effect of polarization carrier separation on the charge-transfer mechanism in the PSCs is elucidated by using the results of ferroelectric and structural studies on the perovskite. The ferroelectric polarization contributes to an inherent carrier-separation effect and the I–V hysteresis. The ferroelectric and semiconducting synergistic charge-separation effect gives an alternative category of solar cells, ferroelectric semiconductor solar cells. Our findings identify the ferroelectric semiconducting behavior of the perovskite absorber as being significant to the improvement of the ferroelectric PSCs performances in future developments.

DOI: 10.1103/PhysRevApplied.6.024007

I. INTRODUCTION

Organic-inorganic perovskite semiconductors have allured massive scientific attention since their incorporation into photovoltaic devices [1–4]. Having a direct band gap and well-aligned energy-band positions at the interfaces, which result in a fast injection of carriers from the perovskite absorber into their respective conductive media, has been reported as the reason for the high efficiencies [3,4]. Transient absorption and photoluminescence-quenching measurements have verified long carrier-diffusion lengths of about 1 μm in mixed halide perovskite ($CH_3NH_3PbI_{(3-x)}Cl_x$) [5] and about 100 nm in $CH_3NH_3PbI_3$ ($MAPbI_3$) [6,7] perovskite by suggesting manipulation of the perovskite absorber material as a promising way to enhance the performances of perovskite solar cells (PSCs).

The pronounced performances together with some unusual characteristics of the PSCs compared to the normal solar cells, such as the current-voltage (I–V) hysteresis [2,8–10], long carrier-diffusion length [5–7], and huge dielectric constant ε [11], hinder to define a clear charge-separation mechanism in the perovskite absorbers. This urges researchers to investigate the fundamental properties of the perovskite absorbers which presumed to be reasons for these mysterious behaviors. Among the fundamental properties, ferroelectricity and ion migration of the perovskite absorber have attracted much interest in the scientific community, since they can generate a polarization on the interfaces of perovskite/TiO_2 and perovskite/HTM which will affect the charge-transfer mechanism in PSCs.

Experimental results and theoretical calculations have suggested the possibility of ferroelectricity of $MAPbI_3$ perovskite [12–16]. Ferroelectric domains about 100 nm in size have been observed by using piezoforce microscopy and ferroelectric domain switching has also been achieved by poling [17]. Larger spontaneous polarizations have been seen in larger perovskite crystals with an external electric field and the retention of ferroelectric polarizations has also been observed after the removal of the electric field; larger crystals have showed longer retention behavior compared with the smaller [18]. A 180° domain phase switching on the $MAPbI_3$ thin films has been observed in PSCs [19]. On the contrary, a few studies have demonstrated the absence of ferroelectricity [20,21]. Xiao *et al.* have excluded the

*Corresponding author.
feng@eng.kagawa-u.ac.jp
†sewvandiga@yahoo.com

contribution of the ferroelectric property due to the absence of polarization-electric field (*P*-*E*) loops and domains [22].

On the other hand, ion migration has also been suggested to be an important factor contributing to the mysterious behaviors. Eames *et al.* have suggested hybrid halide perovskites are mixed ionic-electronic conductors [23]. Yang *et al.* have found low-ionic conduction and high-electronic conduction of $MAPbI_3$ under illumination [24]. First-principles computational analyses carried out on the tetragonal $MAPbI_3$ perovskite and on its interface with TiO_2, have demonstrated the iodine vacancies and interstitials may easily diffuse across the perovskite crystal [25]. Two studies have explained how ferroelectriclike hysteresis can arise from conductive effects and the relation to the *I*–*V* hysteresis in PSCs [20,21].

Numerous studies have been reported on the issue of *I*–*V* hysteresis. Park and Kim studied the effects of the perovskite crystal size and mesoporous TiO_2 layer thickness on *I*–*V* hysteresis and they have found that the hysteresis is pronounced as it decreases crystal size and mesoporous TiO_2 layer thickness [9]. Chen and co-workers have interpreted the stronger hysteresis effects after the reverse poling of the $MAPbI_3$ layer prior to the *I*–*V* measurement as the effect of remanent polarization in the perovskite film [26]. Snaith *et al.* have suggested three possible causes of hysteresis: (1) The perovskite absorber may have large defect density near the interfaces with TiO_2 and HTM, and these defects could act as traps for electrons and holes—under forward bias conditions and short-circuit conditions, defects cause different conductivities at the interfaces due to charge carries filled traps or empty traps; (2) a slow polarization of the material may occur as a result of ferroelectric properties of the organometal trihalide perovskites; and (3) excess ions (iodide and methylamonium) may be present as interstitial defects, and under working conditions they would be able to migrate to either side of the film with the aid of charge collection [10].

As described above, the polarizations by ion diffusion as well as ferroelectricity can have an effect on the charge-transfer mechanisms in PSCs. Hence, quantitative measurements of polarizations by ion migration and ferroelectricity are crucial to the identification of the major effect. To the best of our knowledge, quantitative measurements of polarizations by ion migration and ferroelectricity have not been reported. Furthermore, most of the reported polarization studies focused on the effect on the *I*–*V* hysteresis. We believe the polarization of the perovskite absorber would also contribute to other behaviors of PSCs, such as the charge separation and charge diffusion in the absorber layer. The determination of polarization in leaky semiconductors is challenging [27]. A few studies have tried to evaluate ferroelectric polarization in perovskite films, but did not succeed [12,20]. This may be due to difficulties in measuring ferroelectric polarizations using thin films because uniform thickness and pinhole-free dense film samples are necessary for accurate ferroelectric measurements.

In this study, we prepare $MAPbI_3$ pellet samples and analyze the ferroelectrics of $MAPbI_3$ using the standard methods for ferroelectric studies. The fundamental ferroelectric parameters and ferroelectric behavior of $MAPbI_3$ are provided quantitatively. It is found that $MAPbI_3$ exhibits an antiferroelectric semiconducting behavior which can be used to promote effective charge separation and charge transferring within the perovskite absorbers by the proper ferroelectrics manipulation. We discuss the ferroelectric semiconducting synergistic charge-separation effect in ferroelectric semiconductor solar cells and contributions of the ferroelectric polarization to *I*–*V* hysteresis. Furthermore, strategies to fabricate high-performance PSCs are also reported.

II. EXPERIMENTAL SECTION

A. Chemicals and reagents

Hydroiodic acid (57% in water), and PbI_2 (98%) were purchased from Sigma-Aldrich. Methylamine (40% in methanol) and *N*,*N*-dimethylformamide (DMF) were bought from Wako. All chemicals and reagents were analytical grade and used as received.

B. Synthesis of $MAPbI_3$ powder

CH_3NH_3I is synthesized by reacting 24 mL of methylamine and 10 mL of hydroiodic acid at 0 °C for 2 h in a rotary evaporator at 120 rpm. The solution is evaporated at 80 °C and the precipitate is washed three times in ethanol followed by diethyl either at room temperature for 30 min. The collected precipitate is dried at 60 °C for 24 h. To obtain $CH_3NH_3PbI_3$ ($MAPbI_3$) powder, the synthesized CH_3NH_3I powder is mixed with PbI_2 at a 1 : 1 mole ratio in DMF solvent at 60 °C for 24 h. The perovskite solution is centrifuged at 4500 rpm for 10 min to remove insoluble particles and then the solution is dried at 60 °C for 24 h.

C. Fabrication of $MAPbI_3$ pellets

$MAPbI_3$ pellets are fabricated for ferroelectric measurements. Synthesized $MAPbI_3$ powder is gently ground into fine powder. This powder is then pressed at room temperature and 10-MPa pressure to produce pellets with a diameter of 10 mm and the thickness in a range of 500–600 μm.

D. Characterization

The structural characteristics and purity of the synthesized powders are investigated using a SHIMADZU XRD-6100 x-ray diffractometer with a Cu Kα ($\lambda = 0.15418$) x-ray tube operated at 40 kV and 30 mA using a step size of 0.004° and a scan speed of 0.1°/min. *P*-*E* hysteresis loops at room temperature and desired

frequencies are obtained by using a standard method for the ferroelectric measurements on a TOYO Corporation FCE3–4 KVSY ferroelectric testing system. Leakage currents are measured by applying an electric field of 23.8 kV/cm. The temperature dependences of the relative permittivity (ε_r) at 1 and 10 kHz and frequency dependence of the ε_r are measured by using an Agilent E4980A precision LCR meter. Differential scanning calorimetry (DSC) is conducted on a NETZSCH DSC 200 F3 at a rate of 10 °C min^{-1} over a temperature range from 0 °C to 150 °C under nitrogen.

III. RESULTS AND DISCUSSION

A. $MAPbI_3$ crystal structural analysis

It is pertinent to evaluate lattice parameters of $MAPbI_3$ to analyze its ferroelectric behavior because ferroelectric behavior of the well-known ferroelectric metal-oxide perovskites, such as $BaTiO_3$ and $Pb(Zr,Ti)O_3$, depends strongly on their crystal parameters. The crystal structural parameters of the synthesized $MAPbI_3$ are measured using powder x-ray diffraction (XRD). All diffraction peaks in the XRD pattern can be indexed into the $I4/mcm$ space group of the tetragonal cell with lattice parameters $\boldsymbol{a} = 8.858$ and $\boldsymbol{c} = 12.657$ Å, as shown in Fig. 1. These lattice parameters are in good agreement with the reported values [28]. The $MAPbI_3$ perovskite exhibits superlattices; thus, one unit cell consists of four ABX_3 compositional units [$4-ABX_3$ unit cell, Fig. 2(a)]. We extract a unit cell containing a single ABX_3 compositional unit [$1-ABX_3$ unit cell, Fig. 2(b)] from the superlattice to get the lattice parameters of the $1-ABX_3$ unit cell. The $1-ABX_3$ unit cell belongs to the $P4mm$ space group of the tetragonal cell with lattice constants $\boldsymbol{a}' = 6.264$ $(= a/\sqrt{2})$ and $\boldsymbol{c}' = 6.329$ Å $(= \boldsymbol{c}/2)$. The larger $\boldsymbol{c}'/\boldsymbol{a}' = 1.010$ value than 1 suggests that a spontaneous polarization is possible in the $1-ABX_3$ unit cell similar to the metal-oxide perovskites. However, the $I4/mcm$ space group is a tetragonal centrosymmetric group; thus, a nonpolar phase. A tetragonal $SrTiO_3$ perovskite with the $I4/mcm$ space group has been reported as an antiferroelectric material [29]; therefore, $MAPbI_3$ perovskite can also be an antiferroelectric material as displayed in Fig. 2.

A rapid rotation of MA^+ at high temperature and a restriction in the rotation at low temperature have been observed using ^1H and ^{14}N NMR spectra [30]. The rapid rotation of MA^+ at high temperature causes a MA^+-disordered structure. The temperature-dependent crystal structure of $MAPbI_3$ as lowering temperature has been attributed to highly ordered MA^+ ions [31]. Computational calculation demonstrates dipolar MA^+-ion reorientation between the faces, corners, or edges of the pseudocubic lattice cages in $MAPbI_3$ crystals with a room temperature residence time of 14 ps [32]. On the contrary, neutron scattering techniques and theoretical analysis have identified a rotational mode of the MA^+ cation with a characteristic relaxation time of ~5 ps at room temperature [33]. These results suggest the MA^+-disordered structure of $MAPbI_3$ perovskite at room temperature, namely, the superlattice structure is due to the ordering of the upside-down spontaneous polarizations, and the spontaneous polarization is due to the displacement of positive and negative charge centroids generated by shifting the position of the Pb(II) ion in the PbI_6 octahedron along the $\boldsymbol{c}'$ axis, similar to the antiferroelectric $SrTiO_3$ perovskite [29].

B. Ferroelectric characterization of $MAPbI_3$

The ferroelectrics of $MAPbI_3$ perovskite can be confirmed from its P-E hysteresis loops. The $MAPbI_3$ perovskite exhibits an expanded P-E hysteresis loop, different

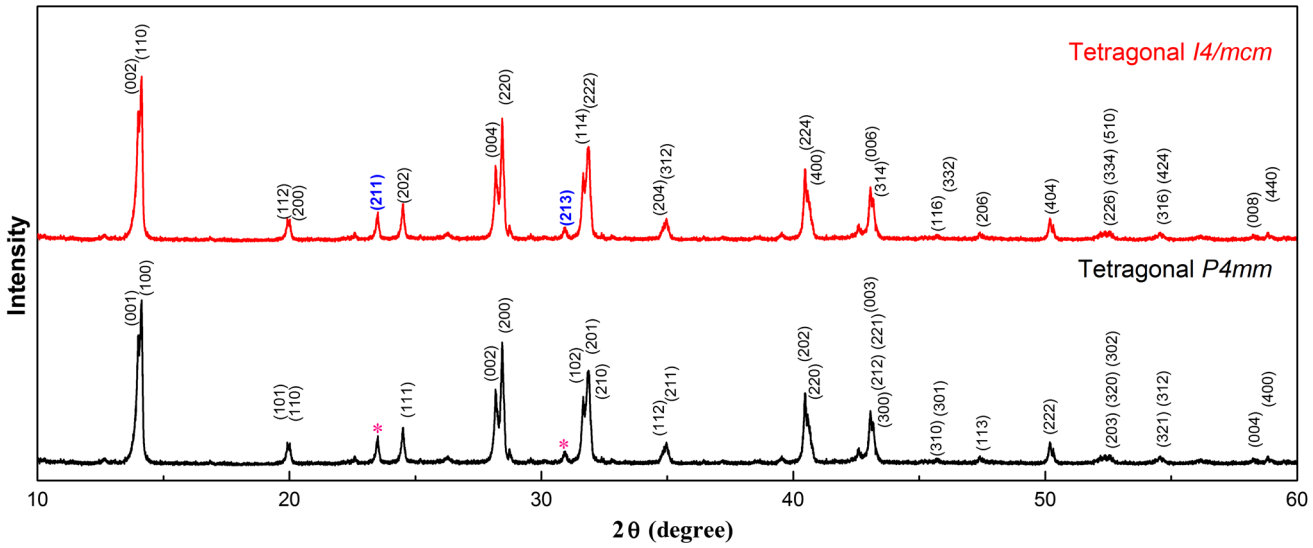

FIG. 1. XRD patterns of $MAPbI_3$ perovskite indexed into tetragonal $I4/mcm$ and $P4mm$ structures.

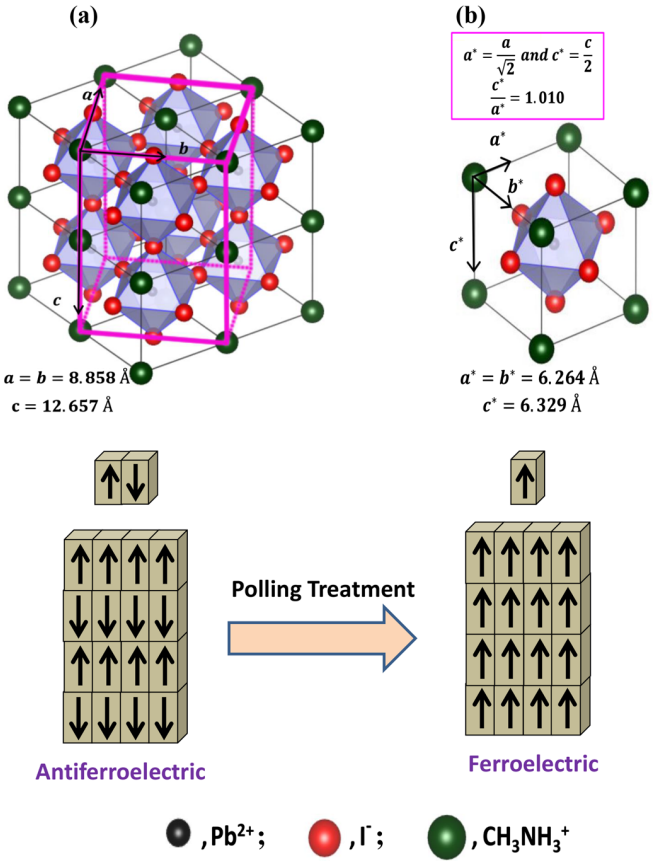

FIG. 2. Relationship of antiferroelectric and ferroelectric phases for $MAPbI_3$ perovskite: (a) antiferroelectric tetragonal $I4/mcm$ (4-ABX_3 superlattice) unit cell; and (b) ferroelectric tetragonal $P4mm$ (disordered 1-ABX_3) unit cell.

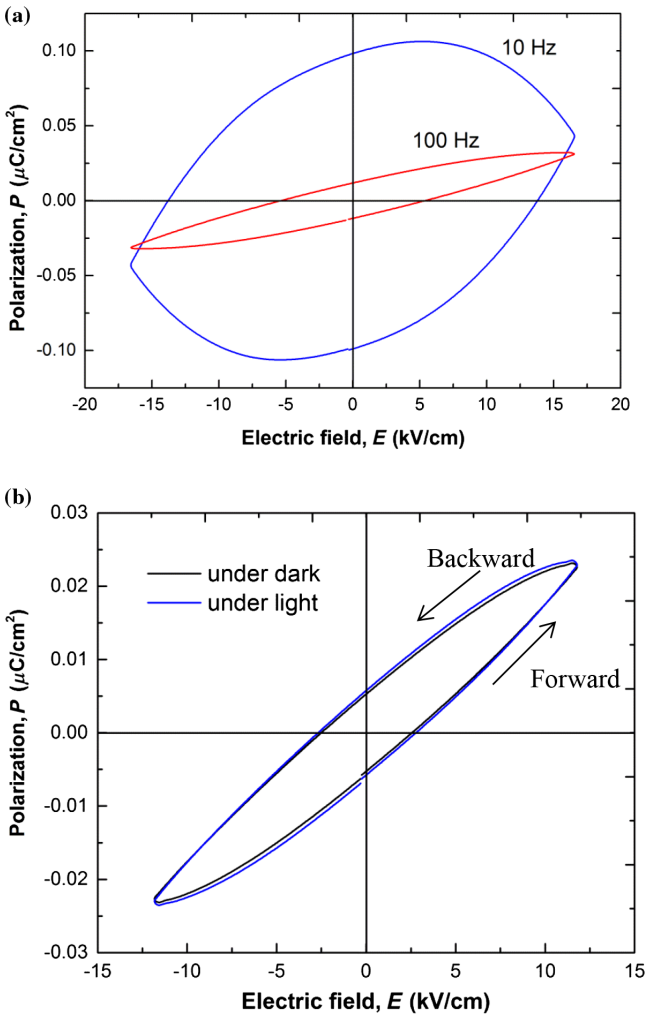

FIG. 3. Polarization-electric field (P-E) hysteresis loops of $MAPbI_3$ perovskite at room temperature: (a) at 10 and 100 Hz; (b) under darkness and light at 100 Hz.

from the typical ferroelectric materials, at the normal measurement frequency of 10 Hz [Fig. 3(a)]. The expanded shape is attributable to the high leakage current [27]. The leakage-current density is 3.7×10^{-6} A/cm^2 under darkness and increases to 8.5×10^{-6} A/cm^2 under illumination at an applied voltage of 23.8 kV/cm (see Fig. 1 in the Supplemental Material [34]). The increase of the leakage current under illumination causes greatly expanded P-E hysteresis loops (see Fig. 2 in the Supplemental Material [34]). The resistivity of 4.51×10^7 and 3.28×10^7 Ωm can be estimated from the leakage currents under darkness and illumination, respectively, which is close to the insulator's resistivity 10^8 Ωm, but smaller than that of the normal ferroelectric materials. The influence of the leakage current can be removed partially by measuring the P-E hysteresis loops at 100 Hz. The almost entire overlap between the P-E hysteresis loops under darkness and illumination at 100 Hz reveals that the influence of the leakage current is negligible [Fig. 3(b)]. Yet, the unsaturated P-E hysteresis loops can be attributed to the low density of the pellet samples prepared at room temperature and ferroelectric $BaTiO_3/SrTiO_3$ synthesized at 900 °C has also displayed the similar shaped P-E loops [35]. Almost no changes in the P-E loops of other similar samples at the same conditions clearly confirm the repeatability of ferroelectric measurements (see Fig. 3 in the Supplemental Material [34]).

The above results indicate that $MAPbI_3$ perovskite shows a ferroelectric semiconducting behavior. A ferroelectric semiconducting material is a semiconductor with a spontaneous polarization, different from the typical ferroelectric materials which are insulators with spontaneous polarizations [36]. It has been reported that some perovskites with $I4/mcm$ space group such as $SrTiO_3$ and $SrTaO_2N$ show ferroelectric behavior due to their antiferroelectrics and local dipoles [37–39]. These perovskites show complex ferroelectric behaviors. The nonpolar antiferroelectric phases, for example $AgNbO_3$ and $NaNbO_3$, can be switched to ferroelectric phases after poling treatment, and these perovskites are used as ferroelectric materials [40,41]. This phenomenon in relation to $MAPbI_3$ perovskite is depicted in Fig. 2. The results of neutron diffraction

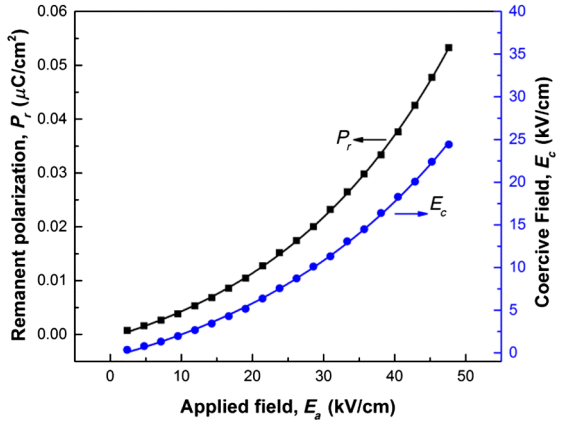

FIG. 4. Changes of remanent polarization and coercive field with applied electric field for MAPbI$_3$.

studies have also suggested the possibility of formation of either antiferroelectric or ferroelectric domains in MAPbI$_3$ perovskite with reducing the temperature based on the ordered orientation of the MA^+ cation [42,43]. However, the MA^+ cation is highly disordered around room temperature, which excludes the possibility of the spontaneous polarization of antiferroelectricity or ferroelectricity by an ordered orientation of the MA^+ cation in the perovskite around room temperature. Except the ordered orientation of the MA^+ cation, the spontaneous polarization is also possible by the displacement of positive and negative charge centroids generated by shifting the position of the Pb(II) ion in the PbI$_6$ octahedron along the c' axis, and also by the displacement of the MA^+ cation position in the organic-inorganic perovskites similar to the most ferroelectric and antiferroelectric metal-oxide perovskites [44–46]. The structural study has indicated that the MA^+ cation is displaced slightly off center of the tetragonal unit cell [47]. Moreover, straightening of the Pb—I—Pb bond angle with increasing temperature from the tetragonal phase to the cubic phase and the distortions of PbI$_6$ octahedra from the ideal have been reported too [43].

Figure 4 shows the variation of remanent polarization and the coercive field with an applied electric field for MAPbI$_3$. As an antiferroelectric material, MAPbI$_3$ shows the increases of remnant polarization and the coercive field with an increasing applied electric field in the measurement range of the applied electric field. Similar behavior has been observed for antiferroelectric materials, such as NaNbO$_3$ [48]. In the measurement range of the applied electric field, where the switching antiferroelectric phase to the ferroelectric phase is dominant, the fraction of the ferroelectric phase in the sample increases with an increasing applied electric field, which causes an increasing remnant polarization and coercive field. We think that at a very high applied electric field, it must show a saturation of polarization. However, at high applied electric field conditions, the sample is broken due to the large leakage current. The measurement of ferroelectric properties in semiconductors is a big challenge.

C. Dielectric characterization of MAPbI$_3$

Dielectric characterizations are performed to compare the dielectric behavior of MAPbI$_3$ perovskite with that of the typical ferroelectric metal-oxide perovskites. Figure 5(a) shows the temperature dependence of the ε_r of MAPbI$_3$ measured at 1- and 10-kHz frequencies. The MAPbI$_3$ perovskite displays a maximum ε_r around 55 °C in a temperature range of 20–70 °C. This temperature corresponds to its Curie temperature (T_c), where the structural phase transitions from the superlattice antiferroelectric tetragonal structure to the paraelectric cubic structure. Dielectric properties of MAPbI$_3$ have already been carried out at low temperatures and the results reveal that the MA^+ ion has a permanent dipole moment, and thus a dynamic process changing the orientation of the ion contributes to the dielectric properties of MAPbI$_3$ [49–51]. Figure 5(b) shows the DSC plot of the MAPbI$_3$ sample where heating and cooling curves show peaks at 58.1 and 55.1 °C, respectively, which correspond to the phase transition. The T_c (= 56.6 °C) calculated from the DSC result is in concurrence with the previously reported value of 54.4 °C [28]. The ε_r is 80 at room temperature and 200 at the T_c at a frequency of 1 kHz. The dielectric behavior with the maximum ε_r at T_c is a feature of ferroelectric metal-oxide perovskites [36].

Figure 6 shows frequency dependence of the ε_r of MAPbI$_3$ under darkness at room temperature. With an increasing frequency (f), the ε_r of MAPbI$_3$ perovskite decreases greatly in the f range of 20–50 Hz (1), shows a shoulder in the f range of 50–100 Hz (2), decreases greatly again above 100 Hz in the range (3), and finally becomes constant in the high f range (4). The ε_r behavior above 100 Hz is similar to the typical ferroelectric materials; thus, the ε_r decreases greatly with increasing frequency in the low-frequency range (Fig. 6) [41,42]. The large frequency dependence in the f range (1) (below 50 Hz) can be attributed mainly to ion migration [52]. The polarization in a ferroelectric material with ion migration P will include a polarization component of ion migration P_{ion}, a spontaneous polarization or ferroelectric component P_{sp}, and a paraelectric polarization component P_{para}, where $P = P_{\text{ion}} + P_{\text{sp}} + P_{\text{para}}$. The $\boldsymbol{\varepsilon}$ can also be separated into $\boldsymbol{\varepsilon} = \boldsymbol{\varepsilon}_{\text{ion}} + \boldsymbol{\varepsilon}_{\text{sp}} + \boldsymbol{\varepsilon}_{\text{para}}$. The $\boldsymbol{\varepsilon}_{\text{ion}}$ and $\boldsymbol{\varepsilon}_{\text{sp}}$ exhibit slow responses, while the $\boldsymbol{\varepsilon}_{\text{para}}$ exhibits a quick response to the applied electric field.

For the ferroelectric materials, the value of $\boldsymbol{\varepsilon}$ decreases as the frequency increases and becomes a constant value at high frequencies, which can be explained by using dipoles oscillating in an alternating electric field as follows [53]. At the low f range (2) ($1/f \gg \tau$, τ is the relaxation time of ferroelectric dipole), dipoles follow the alternating field because they have enough time to respond to the alternating field; namely, P_{sp} can respond to the alternating field and

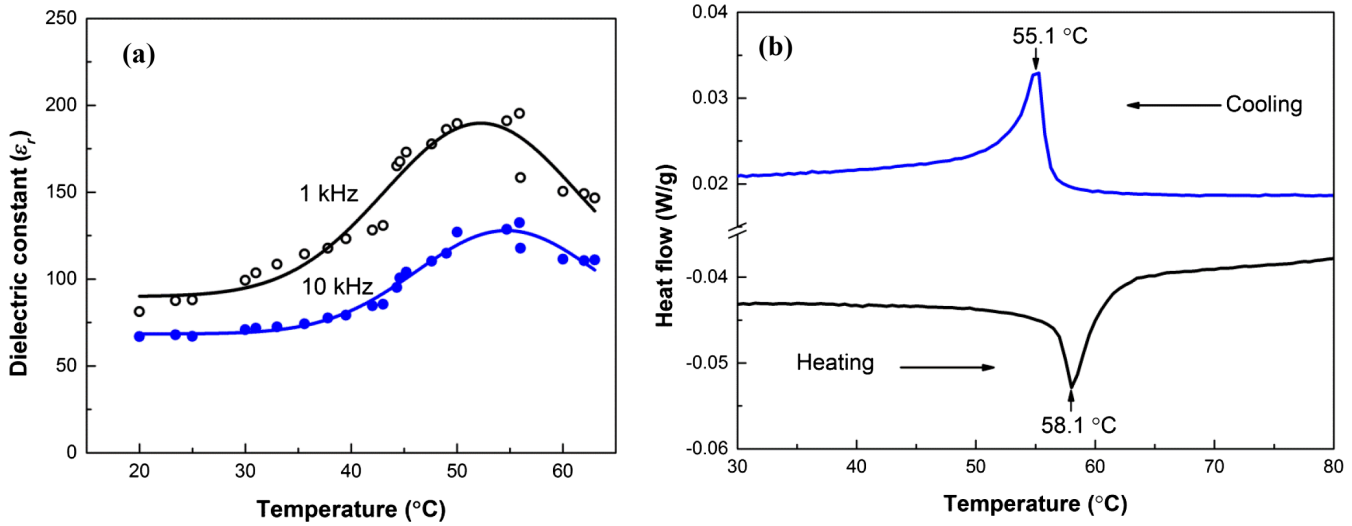

FIG. 5. Dielectric behavior and corresponding phase transition of MAPbI$_3$ perovskite: (a) temperature dependences of relative permittivity measured at 1 and 10 kHz, respectively; (b) DSC plot showing the tetragonal to cubic transition.

gives a large $\boldsymbol{\varepsilon}_{sp}$ value. With increasing f, in the f range (3) ($1/f < \tau$), dipoles begin to lag behind the alternating field and the $\boldsymbol{\varepsilon}_{sp}$ value drops (relaxation process). In the high-f range (4) ($1/f \ll \tau$), dipoles can no longer follow the alternating field and the $\boldsymbol{\varepsilon}_{sp}$ value approaches zero [53]. Since the τ value of P_{para} is much shorter than P_{sp}, the f dependence is very small even at the high f conditions. This is the reason why the ferroelectric materials display large frequency dependence of the $\boldsymbol{\varepsilon}$ at low-frequency conditions. The τ value of P_{ion} should be longer than P_{sp}, and then $\boldsymbol{\varepsilon}_{ion}$ approaches zero even in a very low f range because of a long-distance displacement of ion migration.

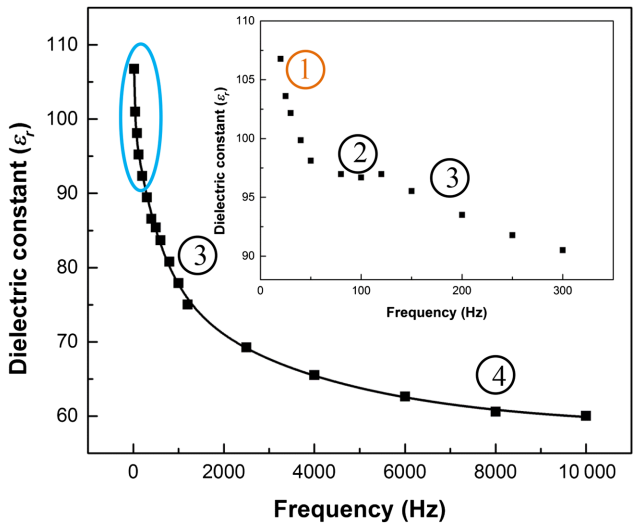

FIG. 6. Frequency dependence of the relative permittivity of $CH_3NH_3PbI_3$ under darkness.

The dielectric result suggests that the ion migration in MAPbI$_3$ perovskite is possible at very low-frequency conditions (below 50 Hz). In the present study, we measure P-E loops at high frequencies to eliminate the effects of ion migration on the ferroelectric polarization. Some studies have suggested the polarization is due to the ion migration. However, the P-E hysteresis loops can be observed even at very high-frequency conditions (see Fig. 4 in the Supplemental Material [34]). The ion displacements can be classified into ion migration (long-distance displacement) and ferroelectric displacement (short-distance displacement). In the case of ferroelectric displacement, the ion displacement can be estimated as about 0.065 Å from the difference of lattice parameters of c' and a' (6.329–6.264 Å) because the ferroelectric displacement may correspond to the shifting the position of Pb(II) ion in the PbI$_6$ octahedron along the c' axis. In the case of the ion migration, the migration distance is much larger than the case of the ferroelectric ion displacement. For example, if the I^- ion is the migration ion, an I^- ion will move at least from its original site to a neighbor I^- site, therefore, a migration distance would be larger than 4 Å. The migration distance of MA^+ would be similar. Hence, the ion-migration polarizations exhibit a slow response to an applied electric field under high-frequency measurement condition. On the other hand, if the leakage current due to electron movement is high, it is difficult to obtain P-E loops. Therefore, we think the effects of electron and ion conductive polarizations would not have an impact on our results.

The origin of ferroelectric spontaneous polarization P_{sp} in the MAPbI$_3$ perovskite can be different from the typical oxide perovskites. It is well known that the P_{sp} of tetragonal $BaTiO_3$ is due to the displacement of positive and negative charge centroids generated by shifting the

position of the Ti(IV) ion in the TiO_6 octahedron along the ***c*** axis, where the deviation of the c/a ratio from unity can be used as an indication of the presence of the ferroelectric phase of $BaTiO_3$. The $\boldsymbol{c}'/\boldsymbol{a}'$ ratio (1.010) of the $MAPbI_3$ perovskite is equal to that of $BaTiO_3$ (1.010) [52]. However, except for a positional shift of the Pb(II) ion in the PbI_6 octahedron, the ordered orientation of asymmetrical MA^+ cations can also cause a displacement of the positive and negative charge centroids in the $MAPbI_3$ perovskite, especially at low temperature [54].

A few studies have demonstrated the absence of ferroelectricity in $MAPbI_3$ perovskite [20,21,22]. This may be due to the formation of a paraelectric pseudocubic phase of $MAPbI_3$ perovskite. It is well known that $BaTiO_3$ perovskites prepared by low temperature processes such as hydrothermal and sol-gel processes have the pseudocubic structure and the pseudocubic $BaTiO_3$ perovskites show paraelectric behavior below the T_c [35,36,52,53]. Reasons for the formation of the pseudocubic $BaTiO_3$ phase are the lattice defects, low crystallinity, and small crystal sizes. Therefore, the formation of the paraelectric pseudocubic $MAPbI_3$ phase is also possible due to the lattice defects, low crystallinity, and small crystal sizes. The structural analysis is important to confirm if the sample used is the paraelectric cubic phase or the tetragonal antiferroelectric phase before discussion of the ferroelectrics of the $MAPbI_3$ phase. In the present study, the tetragonal $MAPbI_3$ phase is used; therefore, we believe the conclusion of antiferroelectrics or ferroelectrics is rational.

D. Charge-separation mechanism of ferroelectric semiconductor solar cells

The ferroelectric carrier-separation effect has been observed in ferroelectric metal oxides and organic materials after poling treatment [55,56]. The ferroelectric $BiFeO_3$ perovskite has shown great potential in photovoltaic applications owing to large photovoltage exceeding several times the band gap or switchable photocurrent [57]. It has been recognized that the ferroelectrics could affect the charge-transfer mechanism in PSCs [18]; however, a comprehensive explanation has not been reported. In our view, solar cells can be categorized as ferroelectric, semiconductor *p-n* junction, and an alternative category; thus, ferroelectric-semiconducting solar cells as shown in Fig. 7. In the ferroelectric solar cell, a poled ferroelectric material, such as ferroelectric metal oxides and organic ferroelectric materials, absorbs photons with energies above the band gap, generates photoelectrons and holes, and then separates photogenerated electrons and holes into contacts by the ferroelectric polarization [Fig. 7(a)] [55,56]. In the semiconductor *p-n* junction solar cell [Fig. 7(b)], photogenerated electrons and holes in the semiconducting absorber layer are separated according to the contacts due to the potential difference at the interfaces (perovskite/TiO_2 and perovskite/HTM).

In the ferroelectric semiconductor solar cell [Fig. 7(c)], the ferroelectric semiconducting absorber layer absorbs photons with energies above the band gap, and generates a photoinduced voltage similar to that of the semiconductor solar cell [Fig. 7(b)], and then the absorber layer is applied by an internal-electric field. If the PSC with 300-nm-thick perovskite film has an open-circuit potential (V_{oc}) of 0.9 V [8], the photoinduced internal-electric field will be 30 kV/cm. This electric field is enough to pole the $MAPbI_3$ perovskite absorber layer (Fig. 4). Namely, the antiferroelectric perovskite absorber layer can be switched to the ferroelectric phase and polarized by the photoinduced voltage of PSCs. We call this polarization behavior a self-poling effect because the polarization is generated by the photoinduced voltage of the PSC without an externally applied electric field. Photogenerated electrons and holes can be separated effectively to the positive and negative faces, respectively, by self-polarization, which contributes to the fast injection of carriers from the perovskite absorber into the TiO_2 and HTM, respectively [3,4]. These findings are consistent with the polarization observations from

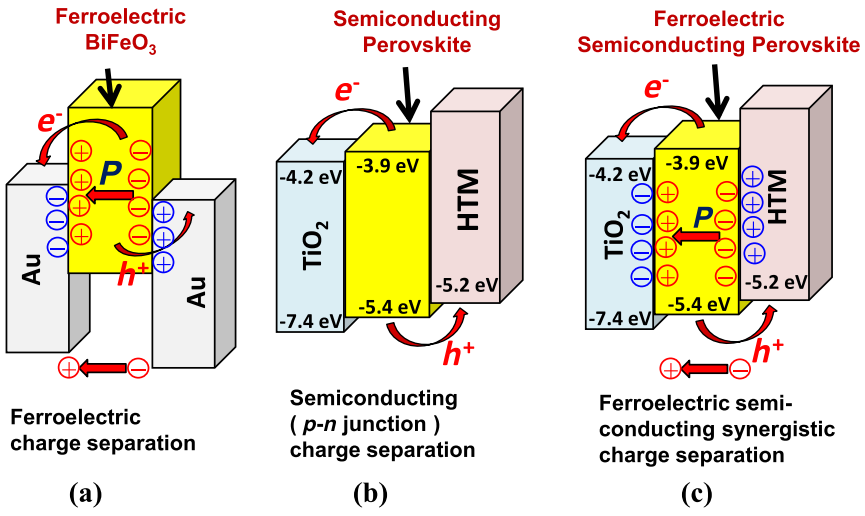

FIG. 7. Charge separation mechanisms in (a) ferroelectric solar cells, (b) semiconductor solar cells, and (c) ferroelectric semiconductor solar cells.

piezoforce microscopy images of positively poled perovskite films [18]. This ferroelectric charge-separation effect is similar to the poling-treated ferroelectric metal oxides and organic materials in the ferroelectric solar cells [35,56]. However, the poling treatment is not necessary for the ferroelectric semiconducting PSCs due to the self-poling effect by the photoinduced internal-electric field, which ingeniously improves the charge-separation effect in the ferroelectric semiconducting PSCs. Because the initial photoinduced internal-electric field is generated by the semiconducting behavior of the perovskite absorber layer, the synergistic effect of ferroelectric and semiconducting behavior is important to give the excellent charge-separation effect.

As it is also possible to generate a polarization by the ion diffusions under the self-poling conditions by the photoinduced internal-electric field in the PSCs, the ion migration polarization can also act similar to the ferroelectric polarization to promote the charge separation as shown in Fig. 7(c). The ferroelectric polarization is reversible as shown in Figs. 3 and 5 in the Supplemental Material [34], when the bias is changed from a forward direction to a backward direction, due to the short-distance ion displacements in the perovskite structure, while the polarization generated by the ion diffusions would show an irreversible or partially reversible behavior because of the long-distance ion diffusions. The ferroelectric displacement is much shorter than that of the ion migration as discussed above. Thus, ferroelectric polarization can occur much more easily and shows much better reversibility than the ion diffusion polarization.

The result of Fig. 3 shows the reversible polarization in the *P-E* loops, which suggests that the polarization would be mainly due to ferroelectric polarization because of the high purity of the sample. It has been reported that high purity, large crystal size, and high crystallinity, which correspond to the high ferroelectricity and low ion-migration ability, are preferred for the high-performance PSCs [9,18]; hence, we think the main polarization contributed to the high-performance PSCs may be due to the ferroelectrics. Nonetheless, a quantitative measurement of ion migration polarization is also necessary to extract the major contribution to the polarization, as the quantitative result for the ferroelectric polarization is given in the present study; however, the quantitative result for the ion-migration polarization has not been reported.

E. Ferroelectric polarization contribution to *I—V* hysteresis

Differences in the shape of the current-voltage (*I–V*) curve in the forward [scanning from short-circuit voltage ($V = 0$) to V_{oc}] and backward (scanning from V_{oc} to 0) directions are manifest as hysteresis in the *I–V* curves. Several difference views have been published on this issue [8–10,26]. We believe the hysteresis is mainly due to the antiferroelectric characteristics of $MAPbI_3$ absorber layer; namely, hysteresis polarization and large ε_r. As described above, the $MAPbI_3$ absorber layer exhibits the ferroelectric polarization charge-separation effect. This ferroelectric charge-separation effect in the forward scanning is different to that in the backward scanning due to the ferroelectric hysteresis behavior of *P-E* as shown in Fig. 3); hence, the charge-separation process also exhibits a hysteresis behavior, namely the larger polarization effect in the backward scanning than that in the forward scanning, which leads to performance variations. In other words, in the forward scanning the main charge separation is due to the semiconducting *p-n* junction effect, while in the backward scanning there is the ferroelectric and semiconducting synergistic effect. That is one of the reasons why the ferroelectric PSCs show the hysteresis in the *I–V* curves.

In addition to the polarization charge-separation effect, the large ε_r of the perovskite can also induce the *I–V* hysteresis because the PSC can act as a capacitor on the *I–V* measurement [9]. To explain the contribution of ε_r on the hysteresis, an equivalent circuit model can be used for perovskite solar cells to represent the *I–V* curve as illustrated in Fig. 8. A resistor R_2, and a capacitor C_{cell} stand for the resistance and capacitance of the cell. The cell capacitance C_{cell} is defined by

$$C_{cell} = \frac{\varepsilon_r \varepsilon_0 A}{d}, \tag{1}$$

where A is the area of the parallel plates, and d is the thickness of the perovskite layer. Generally, open-circuit potentials (V_{oc}) and the absorber layer ($MAPbI_3$) thickness of the perovskite solar cells are in ranges of 0.8–1.0 V and 300–400 nm, respectively [8,26,56]. By assuming the thickness of the $MAPbI_3$ film as 300 nm, the R_2 and C_{cell} can be estimated as $1.35 \times 10^5\ \Omega/cm^2$ and $3.0 \times 10^{-5}\varepsilon_r\ F/m^2$, respectively. In the forward scanning, $J_{ph} = J_{out} + J_c + J_d$, where J_{ph}, J_{out}, J_c, and J_d are the photogenerated current density by the cell, the output current density, the current density for charging the capacitor, and the dark-current density, respectively (Fig. 8). If the capacitance C_{cell} is large, it causes a large reduction in the J_{out}. In the backward scanning, $J_{ph} = J_{out} - J_c + J_d$, where $-J_c$ means the reverse-direction (discharging) current of the C_{cell}, which causes enhancement in the J_{out}. Thus, the difference of J_{out} values in

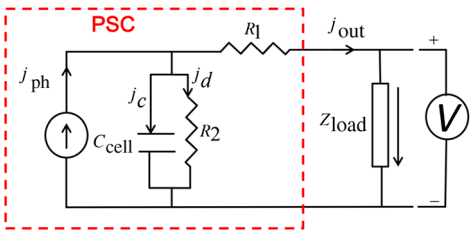

FIG. 8. Equivalent circuit model for perovskite solar cells to represent the *I–V* curve behavior.

forward scanning and backward scanning, $2J_c$, is due to the capacitance, which corresponds to I–V hysteresis. The C_{cell} can be estimated as 3.3×10^{-3} F/m^2 by using $\varepsilon_r = 110$ at 100 Hz in Fig. 6, which suggests that significant hysteresis cannot be expected only from this capacitive effect [58]. It has been reported that the ε_r increases to a very large value of about 10^6 under irradiation and low-frequency conditions [12]. In that case the cell capacitor would give a significant hysteresis.

The hysteresis is also dependent on the cell structure. The mesoporous-TiO_2 electrode exhibits less hysteresis than the planar-TiO_2 electrode [26]. The mesoporous space limits the growth and size of the perovskite crystals in the mesoporous layer. The ferroelectricity of ferroelectric crystal decreases markedly with decreasing the crystal size when the crystal size is smaller than 100 nm [59]. Therefore, the mesoporous-TiO_2 electrode shows less ferroelectric charge-separation effect. That is a reason why the mesoporous-TiO_2 electrode exhibits less hysteresis than the planar-TiO_2 electrode. The smaller crystal size would give a larger ion migration because the ions near the crystal surface exhibit larger ion conductivity than in the bulk crystal. If the ion migration is the main reason of the polarization, the mesoporous-TiO_2 electrode would exhibit larger hysteresis than the planar-TiO_2 electrode. It suggests that the main polarization is due to ferroelectricity.

F. Strategies to fabricate high-performance ferroelectric semiconductor PSCs

On the basis of the above results and discussion, some strategies to fabricate the cells with further enhanced performances can be defined. It is well known that the ferroelectric materials exhibit strong crystal-axis anisotropism. As an example, the spontaneous polarization direction of tetragonal perovskite is in the $\boldsymbol{c}'$-axis direction as shown in Fig. 2(b), and ε_r in the $\boldsymbol{c}'$-axis direction is smaller than that in the $\boldsymbol{a}'$- or $\boldsymbol{b}'$-axis directions [60]. Therefore, an excellent charge-separation effect by the spontaneous polarization could be achieved by using {001}-oriented films. In fact, many reported high-performance perovskite cells have {002}- or {110}-oriented perovskite films [61–63]. Because the direction of spontaneous polarization is switchable, the polarization of the absorber layer by the self-poling effect or an external electric field could improve the cell performances. Generally, fabrication of an oriented film on a polycrystalline substrate is not easy. The topochemical structural conversion is an effective method to fabricate an oriented perovskite film on a polycrystalline substrate by using an intermediate with a layered structure [64]. Fortunately, some intermediates with layered structures, such as PbI_2, $PbI_2(DEMSO)_2$ and $(MA)_2PbI_4$, have been reported in the formation process of $MAPbX_3$ perovskites [61,63,65]. Indeed, the oriented perovskite films from these layered intermediates have been used unconsciously in the perovskite solar cells.

IV. CONCLUSION

The relationship between structure and ferroelectrics of $MAPbI_3$ perovskite is analyzed. The $MAPbI_3$ perovskite is an antiferroelectric semiconductor different from the typical semiconducting materials. The pellet results can be used to estimate the ferroelectric behavior of the perovskite films in the PSCs under their operating conditions. The ferroelectric and semiconducting synergistic effect of the perovskite can be used to promote effective charge separation and charge transferring within the perovskite absorbers by the proper ferroelectricity manipulation. The ferroelectric behavior also contributes to the I–V hysteresis in the PSCs. The clear understanding of the perovskite absorber material is imperative for future developments in the ferroelectric PSCs and the manipulation of ferroelectricity of the absorber materials is a promising strategy to optimize the cell performances.

ACKNOWLEDGMENTS

This work was supported by The Iwatani Naoji Foundation's Research Grant and Grants-in-Aid for Scientific Research (B) (No. 26289240) from Japan Society for the Promotion of Science.

[1] A. Kojima, K. Teshima, Y. Shirai, and T. Miyasaka, Organometal halide perovskites as visible-light sensitizers for photovoltaic cells, J. Am. Chem. Soc. **131**, 6050 (2009).
[2] M. D. McGehee, Perovskite solar cells: Continuing to soar, Nat. Mater. **13**, 845 (2014).
[3] H.-S. Kim, C.-R. Lee, J.-H. Im, K.-B. Lee, T. Moehl, A. Marchioro, S.-J. Moon, R. Humphry-Baker, J.-H. Yum, J. E. Moser, M. Grätzel, and N.-G. Park, Lead iodide perovskite sensitized all-solid-state submicron thin film mesoscopic solar cell with efficiency exceeding 9%, Sci. Rep. **2**, 591 (2012).
[4] P. P. Boix, K. Nonomura, N. Mathews, and S. G. Mhaisalkar, Current progress and future perspectives for organic/inorganic perovskite solar cells, Mater. Today **17**, 16 (2014).
[5] G. Xing, N. Mathews, S. Sun, S. S. Lim, Y. M. Lam, M. Grätzel, S. Mhaisalkar, and T. C. Sum, Long-range balanced electron and hole-transport lengths in organic-inorganic $CH_3NH_3PbI_3$, Science **342**, 344 (2013).
[6] S. D. Stranks, G. E. Eperon, G. Grancini, C. Menelaou, M. J. P. Alcocer, T. Leijtens, L. M. Herz, A. Petrozza, and H. J. Snaith, Electron-hole diffusion lengths exceeding 1 micrometer in an organometal trihalide perovskite absorber, Science **342**, 341 (2013).
[7] V. Gonzalez-Pedro, E. J. Juarez-Perez, W.-S. Arsyad, E. M. Barea, F. Fabregat-Santiago, I. Mora-Sero, and J. Bisquert, General working principles of $CH_3NH_3PbX_3$ perovskite solar cells, Nano Lett. **14**, 888 (2014).
[8] E. L. Unger, E. T. Hoke, C. D. Bailie, W. H. Nguyen, A. R. Bowring, T. Heumüller, M. G. Christoforod, and M. D. McGehee, Hysteresis and transient behavior in

current–voltage measurements of hybrid-perovskite absorber solar cells, Energy Environ. Sci. **7**, 3690 (2014).

[9] H.-S. Kim and N.-G. Park, Parameters affecting *I–V* hysteresis of $CH_3NH_3PbI_3$ perovskite solar cells: Effects of perovskite crystal size and mesoporous TiO_2 layer, J. Phys. Chem. Lett. **5**, 2927 (2014).

[10] H. J. Snaith, A. Abate, J. M. Ball, G. E. Eperon, T. Leijtens, N. K. Noel, S. D. Stranks, J. T.-W. Wang, K. Wojciechowski, and W. Zhang, Anomalous hysteresis in perovskite solar cells, J. Phys. Chem. Lett. **5**, 1511 (2014).

[11] E. J. Juarez-Perez, R. S. Sanchez, L. Badia, G. Garcia-Belmonte, Y. S. Kang, I. Mora-Sero, and J. Bisquert, Photoinduced giant dielectric constant in lead halide perovskite solar cells, J. Phys. Chem. Lett. **5**, 2390 (2014).

[12] C. C. Stoumpos, C. D. Malliakas, and M. G. Kanatzidis, Semiconducting tin and lead iodide perovskites with organic cations: Phase transitions, high mobilities, and near-infrared photoluminescent properties, Inorg. Chem. **52**, 9019 (2013).

[13] J. M. Frost, K. T. Butler, F. Brivio, C. H. Hendon, M. Schilfgaarde, and A. Walsh, Atomistic origins of high-performance in hybrid halide perovskite solar cells, Nano Lett. **14**, 2584 (2014).

[14] J. M. Frost, K. T. Butler, and A. Walsh, Molecular ferroelectric contributions to anomalous hysteresis in hybrid perovskite solar cells, APL Mater. **2**, 081506 (2014).

[15] F. Zheng, H. Takenaka, F. Wang, N. Z. Koocher, and A. M. Rappe, First-principles calculation of the bulk photovoltaic effect in $CH_3NH_3PbI_3$ and $CH_3NH_3PbI_{3-x}Cl_x$, J. Phys. Chem. Lett. **6**, 31 (2015).

[16] S. Liu, F. Zheng, N. Z. Koocher, H. Takenaka, F. Wang, and A. M. Rappe, Ferroelectric domain wall induced band gap reduction and charge separation in organometal halide perovskites, J. Phys. Chem. Lett. **6**, 693 (2015).

[17] Y. Kutes, L. Ye, Y. Shou, S. Pang, B. D. Huey, and N. P. J. Padture, Direct observation of ferroelectric domains in solution-processed $CH_3NH_3PbI_3$ perovskite thin films, J. Phys. Chem. Lett. **5**, 3335 (2014).

[18] H.-S. Kim, S. K. Kim, B. J. Kim, K.-S Shin, M. K. Gupta, H. S. Jung, S.-W. Kim, and N.-G. Park, Ferroelectric polarization in $CH_3NH_3PbI_3$ perovskite, J. Phys. Chem. Lett. **6**, 1735 (2015).

[19] B. Chen, J. Shi, X. Zheng, Y. Zhou, K. Zhuc, and S. Priya, Ferroelectric solar cells based on inorganic–organic hybrid perovskites, J. Mater. Chem. A **3**, 7699 (2015).

[20] Z. Fan, J. Xiao, K. Sun, L. Chen, Y. Hu, J. Ouyang, K. P. Ong, K. Zeng, and J. Wang, Ferroelectricity of $CH_3NH_3PbI_3$ perovskite, J. Phys. Chem. Lett. **6**, 1155 (2015).

[21] J. Beilsten-Edmands, G. E. Eperon, R. D. Johnson, H. J. Snaith, and P. G. Radaelli, Non-ferroelectric nature of the conductance hysteresis in $CH_3NH_3PbI_3$ perovskite-based photovoltaic devices, Appl. Phys. Lett. **106**, 173502 (2015).

[22] Z. Xiao, Y. Yuan, Y. Shao, Q. Wang, Q. Dong, C. Bi, P. Sharma, A. Gruverman, and J. Huang, Giant switchable photovoltaic effect in organometal trihalide perovskite devices, Nat. Mater. **14**, 193 (2015).

[23] C. Eames, J. M. Frost, P. R. F. Barnes, B. C. O'Regan, A. Walsh, and M. S. Islam, Ionic transport in hybrid lead iodide perovskite solar cells, Nat. Commun. **6**, 7497 (2015).

[24] T.-Y. Yang, G. Gregori, N. Pellet, M. Grätzel, and J. Maier, The significance of ion conduction in a hybrid organic–inorganic lead-iodide-based perovskite photosensitizer, Angew. Chem., Int. Ed. **54**, 7905 (2015).

[25] J. M. Azpiroz, E. Mosconi, J. Bisquert, and F. D. Angelis, Defects migration in methylammonium lead iodide and their role in perovskite solar cells operation, Energy Environ. Sci. **8**, 2118 (2015).

[26] H.-W. Chen, N. Sakai, M. Ikegami, and T. Miyasaka, Emergence of hysteresis and transient ferroelectric response in organo-lead halide perovskite solar cells, J. Phys. Chem. Lett. **6**, 164 (2015).

[27] H. Naganuma, Y. Inoue, and S. Okamura, Evaluation of ferroelectric hysteresis loops of leaky multiferroic $BiFeO_3$ films using a system with a high driving frequency of 100 kHz system, J. Ceram. Soc. Jpn. **118**, 656 (2010).

[28] Y. Kawamura, H. Mashiyama, and K. Hasebe, Structural study on cubic–tetragonal transition of $CH_3NH_3PbI_3$, J. Phys. Soc. Jpn. **71**, 1694 (2002).

[29] S. Na and V. David, First-principles study of ferroelectric and antiferrodistortive instabilities in tetragonal $SrTiO_3$, Phys. Rev. B **62**, 21 (2000).

[30] R. E. Wasylishen, O. Knop, and J. B. Macdonald, Cation rotation in methylammonium lead halides, Solid State Commun. **56**, 581 (1985).

[31] A. Poglitsch and D. Weber, Dynamic disorder in methylammoniumtrihalogenoplumbates (II) observed by millimeter-wave spectroscopy, J. Chem. Phys. **87**, 6373 (1987).

[32] A. M. A. Leguy, J. M. Frost, A. P. McMahon, V. G. Sakai, W. Kochelmann, C. H. Law, X. Li, F. Foglia, A. Walsh, B. C. O'Regan, J. Nelson, J. T. Cabral, and P. R. F. Barnes, The dynamics of methylammonium ions in hybrid organic–inorganic perovskite solar cells, Nat. Commun. **6**, 7124 (2015).

[33] T. Chen, B. J. Foley, B. Ipek, M. Tyagi, J. R. D. Copley, C. M. Brown, J. J. Choi, and S.-H. Lee, Rotational dynamics of organic cations in the $CH_3NH_3PbI_3$ perovskite, Phys. Chem. Chem. Phys. **17**, 31278 (2015).

[34] See Supplemental Material at http://link.aps.org/supplemental/10.1103/PhysRevApplied.6.024007 for a plot of leakage-current density against time under light and darkness, *P-E* hysteresis loops under darkness and light at 10 Hz, repeatability of *P-E* hysteresis loops of antiferroelectric $MAPbI_3$ perovskite.

[35] D. Hu, H. Ma, Y. Tanaka, L. Zhao, and Q. Feng, Ferroelectric mesocrystalline $BaTiO_3/SrTiO_3$ nanocomposites with enhanced dielectric and piezoelectric responses, Chem. Mater. **27**, 4983 (2015).

[36] Z.-G. Ye, *Handbook of Advanced Dielectric, Piezoelectric and Ferroelectric Materials Synthesis, Properties and Applications* (Woodhead Publishing, Cambridge, 2008).

[37] D. Oka, Y. Hirose, H. Kamisak, T. Fukumura, K. Sasa, S. Ishii, H. Matsuzaki, Y. Sato, Y. Ikuhara, and T. Hasegawa, Possible ferroelectricity in perovskite oxynitride $SrTaO_2N$ epitaxial thin films, Sci. Rep. **4**, 4987 (2014).

[38] Y. Kim, P. M. Woodward, K. Z. Baba-Kishi, and C. W. Tai, Characterization of the structural, optical, and dielectric properties of oxynitride perovskites AMO_2N (A = Ba, Sr, Ca; M = Ta, Nb), Chem. Mater. **16**, 1267 (2004).

[39] Y. Hinuma, H. Moriwake, Y. Zhang, T. Motohashi, S. Kikkawa, and I. Tanak, First-principles study on relaxor-type ferroelectric behavior without chemical inhomogeneity in $BaTaO_2N$ and $SrTaO_2N$, Chem. Mater. **24**, 4343 (2012).

[40] T. Zhang, C. Zhang, L. Wang, Y. Chai, S. Shen, Y. Sun, H. Yuan, and S. Feng, Low-temperature phase transition in $AgNbO_3$, J. Am. Ceram. Soc. **97**, 1895 (2014).

[41] D. Fu, T. Arioka, H. Taniguchi, T. Taniyama, and M. Itoh, Ferroelectricity and electromechanical coupling in $(1-x)AgNbO_3 - xNaNbO_3$ solid solutions, Appl. Phys. Lett. **99**, 012904 (2011).

[42] M. T. Weller, O. J. Weber, P. F. Henry, A. M. Di Pumpoac, and T. C. Hansenc, Complete structure and cation orientation in the perovskite photovoltaic methylammonium lead iodide between 100 and 352 K, Chem. Commun. **51**, 4180 (2015).

[43] J. M. Frost and A. Walsh, What is moving in hybrid halide perovskite solar cells?, Acc. Chem. Res. **49**, 528 (2016).

[44] M. B. Smith, K. Page, T. Siegrist, P. L. Redmond, E. C. Walter, R. Seshadri, L. E. Brus, and M. L. Steigerwald, Crystal structure and the paraelectric-to-ferroelectric phase transition of nanoscale $BaTiO_3$, J. Am. Chem. Soc. **130**, 6955 (2008).

[45] S. Na and V. David, First-principles study of ferroelectric and antiferrodistortive instabilities in tetragonal $SrTiO_3$, Phys. Rev. B **62**, 21 (2000).

[46] T. Zhang, C. Zhang, L. Wang, Y. Chai, S. Shen, Y. Sun, H. Yuan, and S. Feng, Low-temperature phase transition in $AgNbO_3$, J. Am. Ceram. Soc. **97**, 1895 (2014).

[47] M. T. Weller, O. J. Weber, P. F. Henry, A. M. D. Pumpoac, and T. C. Hansenc, Complete structure and cation orientation in the perovskite photovoltaic methylammonium lead iodide between 100 and 352 K, Chem. Commun. **51**, 4180 (2015).

[48] S. Yamazoe1, H. Sakurai, T. Saito, and T. Wada, Observation of domain structure in 001 orientated $NaNbO_3$ films deposited on (001) $SrTiO_3$ substrates by laser beam scanning microscopy, Appl. Phys. Lett. **96**, 092901 (2010).

[49] A. Poglitsch and D. Weber, Dynamic disorder in methylammoniumtrihalogenoplumbates (II) observed by millimeter-wave spectroscopy, J. Chem. Phys. **87**, 6373 (1987).

[50] N. Onoda-Yamamuro, T. Matsuo, and H. Suga, Dielectric study of $CH_3NH_3PbX_3$ (X = Cl, Br, I), J. Phys. Chem. Solids **53**, 935 (1992).

[51] M. Maeda1, M. Hattori1, A. Hotta1, and I. Suzuki, Dielectric studies on $CH_3NH_3PbX_3$ (X = Cl and Br) single crystals, J. Phys. Soc. Jpn. **66**, 1508 (1997).

[52] M. B. Smith, K. Page, T. Siegrist, P. L. Redmond, E. C. Walter, R. Seshadri, L. E. Brus, and M. L. Steigerwald, Crystal structure and the paraelectric-to-ferroelectric phase transition of nanoscale $BaTiO_3$, J. Am. Chem. Soc. **130**, 6955 (2008).

[53] R. Tripathi, A. Kumar, C. Bharti, and T. P. Sinha, Dielectric relaxation of ZnO nanostructure synthesized by soft chemical method, Curr. Appl. Phys. **10**, 676 (2010).

[54] A. Dualeh, T. Moehl, N. Tétreault, J. Teuscher, P. Gao, M. K. Nazeeruddin, and M. Grätzel, Impedance spectroscopic analysis of lead iodide perovskite-sensitized solid-state solar cells, ACS Nano **8**, 362 (2014).

[55] T. Choi, S. Lee, Y. J. Choi, Kiryukhin, and S.-W. Cheong, Switchable ferroelectric diode and photovoltaic effect in $BiFeO_3$, Science **324**, 63 (2009).

[56] Y. Funatsu, A. Sonoda, and M. Funahashi, Ferroelectric liquid-crystalline semiconductors based on a phenylterthiophene skeleton: Effect of the introduction of oligosiloxane moieties and photovoltaic effect, J. Mater. Chem. C **3**, 1982 (2015).

[57] W.-Q. Liao, Y. Zhang, C.-L. Hu, J.-G. Mao, H.-Y. Ye, P.-F. Li, S. D. Huang, and R.-G. Xiong, A lead-halide perovskite molecular ferroelectric semiconductor, Nat. Commun. **6**, 7338 (2015).

[58] B. C. O'Regan, P. R. F. Barnes, X. Li, C. Law, E. Palomares, and J. M. Marin-Beloqui, Optoelectronic studies of methylammonium lead iodide perovskite solar cells with mesoporous TiO_2: Separation of electronic and chemical charge storage, understanding two recombination lifetimes, and the evolution of band offsets during *J-V* hysteresis, J. Am. Chem. Soc. **137**, 5087 (2015).

[59] L. Li, P. A. Salvador, and G. S. Rohrer, Photocatalysts with internal electric fields, Nanoscale **6**, 24 (2014).

[60] D. Mayergoyz and G. Bertotti, *The Science of Hysteresis* (Elsevier, London, 2004), Chap. 4.

[61] J. Burschka, N. Pellet, S.-J. Moon, R. Humphry-Baker, P. Gao, M. K. Nazeeruddin, and M. Grätzel, Sequential deposition as a route to high-performance perovskite-sensitized solar cells, Nature (London) **499**, 316 (2013).

[62] M. Liu, M. B. Johnston, and H. J. Snaith, Efficient planar heterojunction perovskite solar cells by vapor deposition, Nature (London) **501**, 395 (2013).

[63] Q. Chen, H. Zhou, Z. Hong, S. Luo, H.-S. Duan, H.-H. Wang, Y. Liu, G. Li, and Y. Yang, Planar heterojunction perovskite solar cells via vapor-assisted solution process, J. Am. Chem. Soc. **136**, 622 (2014).

[64] Q. Feng, K. Kajiyoshi, and K. Yanagisawa, Topotactic preparation of preferentially oriented $BaTiO_3$ and TiO_2 thin films on polycrystalline substrate, Chem. Lett. **32**, 48 (2003).

[65] T. C. Sum and N. Mathews, Advancements in perovskite solar cells: Photophysics behind the photovoltaics, Energy Environ. Sci. **7**, 2518 (2014).